SUPPLEMENTAL METHODS

Participant Recruitment and Assessment

Across all sites, participants underwent a comprehensive clinical battery to assess current internalizing psychopathology and maltreatment history. Diagnoses were made according to DSM-IV criteria using the Kiddie Schedule for Affective Disorders and Schizophrenia (KSADS)(1). All study sites excluded participants with substance dependency or abuse, an unstable medical condition, current use of psychotropic medication, MRI contraindication, or pregnancy. Binary illness assignment (no diagnoses vs. at least one diagnosis) was defined as a current diagnosis of major depressive disorder (MDD), generalized anxiety disorder (GAD), separation anxiety disorder (SAD), or PTSD. Girls meeting diagnostic criteria for past or present psychotic, bipolar, or obsessive-compulsive disorders were excluded from the individual studies outright. Subsets of girls completed the following symptom severity assessments: the Mood and Feelings Questionnaire(2) (MFQ; n=169; Madison, WI cohort completed full version; Little Rock, AK cohorts completed short version; Seattle, WA cohort did not complete) assessing depression symptoms, the Screen for Child Anxiety Related Emotional Disorders(3) (SCARED; n=122; Little Rock, AK cohorts did not complete) assessing anxiety symptoms, and the UCLA PTSD Reaction Index(4) (PTSD-RI; n=134) assessing post-traumatic stress disorder (PTSD) symptoms.

Childhood abuse and neglect were assessed using the Childhood Trauma Questionnaire (CTQ)(5). Abuse severity was measured with the sum of the CTQ abuse subscales. Binary abuse assignment (non-exposed vs. exposed) was defined based on previous validation(6): any subscale greater than 'None' (physical abuse total>7, sexual abuse total>5, and emotional abuse total>8) indicated abuse exposure. Neglect severity was measured with the CTQ physical neglect subscale. Girls were labeled as *Resilient* if they had a history of abuse and no internalizing diagnoses, while girls with abuse exposure and at least one internalizing diagnosis were labeled as *Susceptible*. Finally, girls from the Madison, WI and Seattle, WA cohorts completed the Weschler Abbreviated Scale of Intelligence-II(7) and the Little Rock, AR cohort

completed the Expressive One-Word Picture Vocabulary Test(8), each to assess IQ .The girls from Madison and Seattle also completed the Tanner Stage self-report of pubertal development(9).

Image Acquisition and Individual Preprocessing

Image preprocessing of T1-weighted MRI scans and whole-brain voxel-based morphometry (VBM) was conducted using the Computational Anatomy Toolbox (CAT12; http://dbm.neuro.uni-jena.de/cat/) within Statistical Parametric Mapping software (SPM12; Wellcome Department of Imaging Neuroscience, London, United Kingdom) running on MATLAB 8.3 (Mathworks, Natick, MA, USA). All recommended default parameters within the CAT12 manual were used. The T1-weighted images were first spatially normalized to Montreal Neurological Institute (MNI) template space using the DARTEL algorithm. Next, the images were segmented into gray matter (GM), white matter (WM), and cerebrospinal fluid (CSF) using SPM12 tissue probability maps. A final quality check of the covariance structure of all gray matter images ensured homogeneity. The final voxel resolution was 1 x 1 x 1 mm.

Mean voxel-wise cortical and subcortical GMV estimates were extracted using parcellations from the Brainnetome Atlas(10), while cerebellar regions were extracted from the updated automatic anatomical labeling atlas (AAL2)(11). Both atlases were converted to MNI space for spatial consistency. For the whole-brain analyses, all regions-of-interest (ROIs) were included, yielding a total of 272 ROIs. For the emotion and language circuitry analyses, maps of voxels forming emotion and language circuitry were created in Neurosynth (www.neurosynth.org)(12) with the search terms “emotion” and “language” respectively (top panel of Supplemental Figure S1). Erring on the side of ROI inclusion, the uniformity test was used, and an ROI was included if it showed at least 25% spatial overlap with the Neurosynth mask (bottom panel of Supplemental Figure S1). This yielded a total of 152 and 141 ROIs for emotion and language circuits respectively. These ROI masks had considerable overlap: emotion ROIs showed 77.0% voxel overlap with the language ROIs and the language ROIs showed 77.6% overlap with the emotion ROIs. The specific regions used in each parcellation are listed in Supplemental Table S2. The remaining preprocessing steps were completed in R(13), where each GMV estimate was scaled to total intracranial

volume (TIV). Finally, site-pooled data were harmonized across MR scanners through batch effects correction in *ComBat* (*sva* package)(14), which effectively removed scanner-related differences in GMV ROIs (Supplemental Figure S2). Importantly, abuse and diagnosis assignment, as well as chronological age, were included in the *ComBat* design matrix to ensure variance-of-interest was not removed.

Model Building and Training

Stacked generalization is a form of ensemble machine learning whereby individual, "lower-level" learning algorithms are aggregated to increase predictive power by utilizing the strengths of each base model (referred to as *submodels*). For example, ridge regression models are powerful in linear contexts, generalize well even with smaller sample sizes, but tend to underfit the data because the model cannot detect interactive, non-linear complexities between predictors. Multi-layer perceptron models (artificial neural networks), on the other hand, are ideal for detecting highly-interactive relationships between predictors and make no linear assumptions, however tend to overfit the data, especially when trained with small samples. A "super learner", therefore, is a final prediction aggregation model with the objective of finding the optimal combination of submodel predictions, theoretically accounting for these strengths and weaknesses.

First, a set of machine learning regression submodels underwent hyperparameter tuning using 10-fold cross-validation on the training set (remaining instances after pseudorandom assignment to the validation set; $n = 74$). Next, the super learner's hyperparameters were optimized using submodel held-out predictions during 10-fold cross-validation. Here, the hold-outs were used as "second-order" features (one prediction per submodel, per instance). Then, the optimized super learner and all submodels were trained with the full hold-out set. Once all models were optimized and trained, the super learner was evaluated on the validation set ($n = 24$) as further described below.

Five machine learning algorithms were used as submodels for the prediction of chronological age in TD girls. Submodels' hyperparameters were tuned with 10-fold cross-validation. As many GMV estimates were related, it was important that each submodel algorithm be robust to correlated features. These

algorithms included ridge regression (RR)(15) trained with stochastic gradient descent, support vector machine (SVM) regression(16), multilayer perceptron (MLP)(17), random forest (RF) regression(18), and gradient boosting machine (boosted trees; GBM) regression(19). Super learner coefficients were optimized using an additional RR model (also trained with stochastic gradient descent) excluding an intercept term. All algorithms were implemented in Python (v 3.7.0) using *SciKit-Learn* (20).

Hyperparameter Tuning

Each submodel contained hyperparameters (*a priori* settings/options for particular algorithms) that needed to be specified upon creation. In order to maximize predictive value of each model, a randomized hyperparameter search using 10-fold cross validation was implemented in *SciKit-Learn*. A probability distribution of possible parameter values was chosen *a priori* for each hyperparameter. Random values were drawn from Gaussian distributions (generated with *SciPy* (21)) centered at the recommended value for that parameter, as provided by *SciKit-Learn*'s documentation. If nominal options were given for a parameter, random uniform distributions were used. The search space for each model, as well as their corresponding *SciKit-Learn* functions, are listed in Supplemental Table S3. In the special case of the multilayer perceptron, network architecture was decided *a priori*: a single hidden layer was used containing roughly half the training sample size (40) neurons. Each neuron had a unique bias term and a rectified linear unit (ReLU) activation function. The output layer contained no activation function. Optimized, fully-trained submodels and their super learner coefficients were saved using the Python-based *Joblib* (v. 0.13.2) for subsequent analyses.

Label/Age Bias Correction in Group-Level BrainAGE Analyses

The BrainAGE is a highly non-linear residual, describing the n-dimensional "distance" between the true chronological age and the super learner's prediction. However, as displayed in Supplemental Figure S4, super learner predictions have an "age bias", where the model systemically *over*-estimates BrainAGE for younger girls and *under*-estimates BrainAGE for older girls. Unfortunately, this is extremely common across studies incorporating normative development models, especially those using the BrainAGE

index and likely represents a statistical "regression-to-the-mean" effect (although explaining this bias more rigorously, as well as methods to correct it, are active areas of research). In order to use the BrainAGE as intended, the index should represent the degree of deviation from normative development independent of the true chronological age of the brain being analyzed. For this reason we covary for label (chronological age) in all group-level analyses, ensuring that abuse- and internalizing-related differences in BrainAGE were not attributable to there being younger (or older) girls in one group relative to another.

BrainAGE Group-Level Analyses

Linear mixed-effects models in R (*lme4* package), were used to determine abuse- and diagnosis-related differences in BrainAGE from whole-brain, emotion, and language circuit features. For abuse, we used both binary and continuous approaches to test two related, but distinct questions: first, does having been abused induce advanced maturation in girl's emotion circuitry (binary)? And second, is there a relationship between the amount of abuse a girl has experienced and altered maturation of emotion circuitry (continuous)? To test the first question, we used the binary abuse exposure assignment to explain BrainAGE, but importantly, covaried for abuse load. To test the second question, we used the continuous total CTQ abuse measure to explain BrainAGE, both across all girls (typically-developing + resilient + susceptible) and within only abused girls. Because physical neglect scores did not vary considerably across the sample, binarization was not possible due to extreme class imbalance (no exposure >> exposure). Therefore, only continuous physical neglect was used. Covariates for all analyses included chronological age (to account for super learner label bias), IQ, scanner, and physical neglect experiences.

Post-Hoc Analyses: Symptom Severity Relationships with BrainAGE

BrainAGE relationships with internalizing symptom severity were analyzed to investigate whether significant abuse- or diagnosis-related BrainAGEs may be associated with psychiatric symptoms. An LME model including PTSD, depression, and anxiety symptom totals, as well as the group-level covariates (chronological age, scanner, IQ, physical neglect) was implemented. Abuse severity was also included as a

covariate in these models to ensure symptom-related effects could not be explained by more or less abuse exposure. Because these symptom scores were not collected in all girls (missing not-at-random), analyses were run in girls where data was available. Additionally, a model including subdimensions of DSM-IV PTSD symptoms (re-experiencing, avoidance, hyperarousal) was also tested.

Post-Hoc Analyses: Puberty Relationships with BrainAGE

BrainAGE relationships with pubertal status was analyzed to investigate whether significant abuse- or diagnosis-related BrainAGEs may be related to developmental milestones. More specifically, an LME model including Tanner Stage pubertal score, its interactions with abuse-exposure and diagnosis, and the group-level covariates (label, scanner, IQ, physical neglect) as predictors was implemented. Because Tanner Stage was only collected in a subset of girls (Madison, WI and Seattle, WA cohorts), it was assessed in girls where data was available.

Calculating Regional Influence on BrainAGE

Briefly, for each ROI, 1000 random bootstrap samples of that feature were created from each abuse group (Resilient, Susceptible). For each abuse-related bootstrap, the new feature vector replaced the TD feature vector for only that region, leaving all other TD feature vectors intact. Chronological age was predicted and BrainAGE was re-calculated. Finally, median BrainAGE (across bootstraps) was calculated for each girl, yielding a perturbed BrainAGE distribution for that region. Paired-samples Wilcoxon tests compared the abuse-perturbed BrainAGE distribution to the true BrainAGE distribution. In order to ensure that the abuse-perturbed BrainAGEs indeed changed beyond chance expectations (i.e. the feature was informative for age prediction generally, regardless of phenotype), an additional comparison was made with a TD-perturbed bootstrap for that feature (similar to how the null distribution of model performances was calculated earlier). As hundreds of regions were being tested univariately, a false discovery rate (FDR; implemented in SciPy) correction was applied across Wilcoxon p -values. If the abuse-perturbed BrainAGE distribution was significantly different than both the true BrainAGE distribution and TD-perturbed BrainAGE distribution for that ROI (FDR-corrected $p < 0.05$), then that abuse-related ROI was considered

significantly influential. Finally, if a region was found to be influential, the adjusted effect size (adj. R^2) was calculated and ROIs were segregated based on whether they increased or decreased median BrainAGE.

SUPPLEMENTAL REFERENCES

1. Kaufman J, Birmaher B, Brent D, Rao U, Flynn C, Moreci P, et al. Schedule for Affective Disorders and Schizophrenia for School-Age Children-Present and Lifetime Version (K-SADS-PL): initial reliability and validity data. J Am Acad Child Adolesc Psychiatry. 1997 Jul;36(7):980–8.

2. Costello EJ, Angold A. Scales to assess child and adolescent depression: checklists, screens, and nets. J Am Acad Child Adolesc Psychiatry. 1988 Nov;27(6):726–37.

3. Birmaher B, Khetarpal S, Brent D, Cully M, Balach L, Kaufman J, et al. The Screen for Child Anxiety Related Emotional Disorders (SCARED): scale construction and psychometric characteristics. J Am Acad Child Adolesc Psychiatry. 1997 Apr;36(4):545–53.

4. Steinberg AM, Brymer MJ, Decker KB, Pynoos RS. The University of California at Los Angeles Post-traumatic Stress Disorder Reaction Index. Curr Psychiatry Rep. 2004 Apr;6(2):96–100.

5. Bernstein DP, Fink L, Handelsman L, Foote J, Lovejoy M, Wenzel K, et al. Initial reliability and validity of a new retrospective measure of child abuse and neglect. Am J Psychiatry. 1994 Aug;151(8):1132–6.

6. Bernstein DP, Ahluvalia T, Pogge D, Handelsman L. Validity of the Childhood Trauma Questionnaire in an Adolescent Psychiatric Population. J Am Acad Child Adolesc Psychiatry. 1997 Mar 1;36(3):340–8.

7. Wechsler D. Wechsler Abbreviated Scale of Intelligence–Second Edition Manual. Bloomington, MN: Pearson; 2011.

8. Gardner MF, Academic Therapy Publications, Pro-Ed (Firm), Expressive one-word picture vocabulary test. EOWPVT-R: expressive one-word picture vocabulary test, revised. Novato, Calif.; [Austin, Tex.: Academic Therapy Publications ; [Distributed by Pro-Ed; 1990.

9. Morris NM, Udry JR. Validation of a self-administered instrument to assess stage of adolescent development. J Youth Adolesc. 1980 Jun 1;9(3):271–80.

10. Fan L, Li H, Zhuo J, Zhang Y, Wang J, Chen L, et al. The Human Brainnetome Atlas: A New Brain Atlas Based on Connectional Architecture. Cereb Cortex. 2016 Aug 1;26(8):3508–26.

11. Rolls ET, Joliot M, Tzourio-Mazoyer N. Implementation of a new parcellation of the orbitofrontal cortex in the automated anatomical labeling atlas. NeuroImage. 2015 Nov 15;122:1–5.

12. Yarkoni T, Poldrack RA, Nichols TE, Van Essen DC, Wager TD. Large-scale automated synthesis of human functional neuroimaging data. Nat Methods. 2011 Jun 26;8(8):665–70.

13. R Core Team. R: A Language and Environment for Statistical Computing [Internet]. Vienna, Austria: R Foundation for Statistical Computing; 2016. Available from: https://www.R-project.org

14. Fortin J-P, Cullen N, Sheline YI, Taylor WD, Aselcioglu I, Cook PA, et al. Harmonization of cortical thickness measurements across scanners and sites. NeuroImage. 2018 Feb 15;167:104–20.

15. Hoerl AE, Kennard RW. Ridge Regression: Biased Estimation for Nonorthogonal Problems. Technometrics. 1970;12(1):55–67.

16. Boser BE, Guyon IM, Vapnik VN. A Training Algorithm for Optimal Margin Classifiers. In: Proceedings of the 5th Annual ACM Workshop on Computational Learning Theory. ACM Press; 1992. p. 144–152.

17. Rumelhart DE, Hinton GE, Williams RJ. Learning Internal Representations by Error Propagation [Internet]. CALIFORNIA UNIV SAN DIEGO LA JOLLA INST FOR COGNITIVE SCIENCE; 1985 Sep [cited 2019 Oct 30]. Report No.: ICS-8506. Available from: https://apps.dtic.mil/docs/citations/ADA164453

18. Ho TK. Random Decision Forests. In: Proceedings of the Third International Conference on Document Analysis and Recognition (Volume 1) - Volume 1 [Internet]. Washington, DC, USA: IEEE Computer Society; 1995 [cited 2018 Oct 31]. p. 278–. (ICDAR '95). Available from: http://dl.acm.org/citation.cfm?id=844379.844681

19. Friedman JH. Greedy Function Approximation: A Gradient Boosting Machine. Ann Stat. 2001;29(5):1189–232.

20. Pedregosa F, Varoquaux G, Gramfort A, Michel V, Thirion B, Grisel O, et al. Scikit-learn: Machine Learning in Python. J Mach Learn Res. 2011;12(Oct):2825–30.

21. Virtanen P, Gommers R, Oliphant TE, Haberland M, Reddy T, Cournapeau D, et al. SciPy 1.0-Fundamental Algorithms for Scientific Computing in Python. ArXiv. 2019;abs/1907.10121.

SUPPLEMENTAL TABLES

Supplemental Table S1. Demographic, maltreatment, and clinical variables, as well as scanning parameters, for participants within each study site/cohort. Values, unless otherwise specified, indicate means with standard deviations in parentheses. Ranges are in brackets. TD = typically-developing; CTQ = Childhood Trauma Questionnaire; PTSD = post-traumatic stress disorder; MFQ = Mood and Feelings Questionnaire; SCARED = Screen for Child Anxiety Related Emotional Disorders; PTSD-RI = PTSD Reaction Index
* Indicates a variable that was not consistently available for all subjects. Statistics are provided for data that were available

Study Site	University of Wisconsin			University of Arkansas			University of Washington		
	TD	Resilient	Susceptible	TD	Resilient	Susceptible	TD	Resilient	Susceptible
Demographic Variables									
n	22	5	19	41	30	48	36	15	18
Age	14.63 (2.98) [9.63, 18.60]	14.73 (2.28) [12.36, 17.51]	14.70 (3.23) [8.07, 18.80]	14.32 (2.11) [11.00, 18.00]	14.77 (1.68) [11.00, 17.00]	14.77 (1.73) [11.00, 17.00]	12.63 (2.64) [8.53, 16.97]	12.73 (2.71) [8.53, 16.85]	13.82 (2.58) [8.45, 16.78]
IQ	110.77 (12.16)	105.80 (3.03)	96.39 (10.01)	114.07 (19.31)	99.87 (16.27)	95.81 (16.33)	109.50 (16.01)	118.40 (14.87)	110.61 (13.40)
Tanner Stage				-	-	-			
Maltreatment and Clinical Variables									
CTQ Abuse	15.91 (1.11) [15, 18]	21.6 (1.82) [20, 24]	39.74 (13.37) [19, 70]	15.87 (1.08) [15, 19]	26.77 (9.94) [18, 57]	32.19 (11.89) [19, 75]	16.03 (1.11) [15, 18]	25.67 (5.60) [18, 37]	32.22 (11.26) [19, 64]
CTQ Physical Neglect	5.36 (0.66) [5, 7]	6.80 (1.48) [5, 9]	10.42 (3.93) [5, 22]	8.66 (3.99) [5, 14]	8.73 (3.60) [5, 17]	9.06 (4.18) [5, 23]	5.44 (0.94) [5, 9]	9.47 (3.91) [5, 18]	10.61 (5.49) [5, 23]
Anxiety Disorder (n)	-	-	8	-	-	23	-	-	7
Depressive Disorder (n)	-	-	18	-	-	36	-	-	7
PTSD (n)	-	-	19	-	-	32	-	-	5
MFQ*	-	4.20 (1.60)	28.21 (9.81)	-	4.67 (4.71)	12.58 (6.95)	-	-	-
SCARED*		9.50 (3.92)	38.47 (14.68)	-	-	-	-	23.27 (11.14)	26.89 (16.68)
PTSD-RI*	-	-	58.61 (10.82)	-	18.11 (15.10)	40.73 (16.70)	-	26.13 (15.64)	28.00 (12.31)
Scan Parameters									
Tesla	3T			3T			3T		
Head-Coil	8-Channel			32-Channel			32-Channel		
TE	3.20ms			3.02ms, 3.70ms			3.5		
TR	8.20ms			2.60ms, 7.50ms			2.53ms		

Supplemental Table S2. Regions from the Brainnetome and Automated Anatomical Labelling 2 atlases included in emotion and language circuitry parcellations.

Circuit	Atlas Region ID	Hemisphere	Lobe	Gyrus	Description
Emotion	Amyg_L_2_1	L	Subcortical Nuclei	Amygdala	Medial Amygdala
	Amyg_L_2_2	L	Subcortical Nuclei	Amygdala	Lateral Amygdala
	Amyg_R_2_1	R	Subcortical Nuclei	Amygdala	Medial Amygdala
	Amyg_R_2_2	R	Subcortical Nuclei	Amygdala	Lateral Amygdala
	BG_L_6_1	L	Subcortical Nuclei	Basal Ganglia	Ventral Caudate
	BG_L_6_2	L	Subcortical Nuclei	Basal Ganglia	Globus Pallidus
	BG_L_6_3	L	Subcortical Nuclei	Basal Ganglia	Nucleus Accumbens
	BG_L_6_4	L	Subcortical Nuclei	Basal Ganglia	Ventromedial Putamen
	BG_L_6_5	L	Subcortical Nuclei	Basal Ganglia	Dorsal Caudate
	BG_L_6_6	L	Subcortical Nuclei	Basal Ganglia	Dorsolateral Putamen
	BG_R_6_1	R	Subcortical Nuclei	Basal Ganglia	Ventral Caudate
	BG_R_6_2	R	Subcortical Nuclei	Basal Ganglia	Globus Pallidus
	BG_R_6_3	R	Subcortical Nuclei	Basal Ganglia	Nucleus Accumbens
	BG_R_6_4	R	Subcortical Nuclei	Basal Ganglia	Ventromedial Putamen
	BG_R_6_5	R	Subcortical Nuclei	Basal Ganglia	Dorsal Caudate
	BG_R_6_6	R	Subcortical Nuclei	Basal Ganglia	Dorsolateral Putamen
	CG_L_7_1	L	Cingulate	Cingulate Gyrus	Dorsal Area 23
	CG_L_7_2	L	Cingulate	Cingulate Gyrus	Rostroventral Area 24
	CG_L_7_3	L	Cingulate	Cingulate Gyrus	Pregenual Area 32
	CG_L_7_4	L	Cingulate	Cingulate Gyrus	Ventral Area 23
	CG_L_7_5	L	Cingulate	Cingulate Gyrus	Caudodorsal Area 24
	CG_L_7_7	L	Cingulate	Cingulate Gyrus	Subgenual Area 32
	CG_R_7_1	R	Cingulate	Cingulate Gyrus	Dorsal Area 23
	CG_R_7_2	R	Cingulate	Cingulate Gyrus	Rostroventral Area 24
	CG_R_7_3	R	Cingulate	Cingulate Gyrus	Pregenual Area 32
	CG_R_7_5	R	Cingulate	Cingulate Gyrus	Caudodorsal Area 24
	CG_R_7_7	R	Cingulate	Cingulate Gyrus	Subgenual Area 32
	FuG_L_3_2	L	Temporal	Fusiform Gyrus	Medioventral Area37
	FuG_L_3_3	L	Temporal	Fusiform Gyrus	Lateroventral Area37
	FuG_R_3_2	R	Temporal	Fusiform Gyrus	Medioventral Area37
	FuG_R_3_3	R	Temporal	Fusiform Gyrus	Lateroventral Area37
	Hipp_L_2_1	L	Subcortical Nuclei	Hippocampus	Rostral Hippocampus
	Hipp_L_2_2	L	Subcortical Nuclei	Hippocampus	Caudal Hippocampus
	Hipp_R_2_1	R	Subcortical Nuclei	Hippocampus	Rostral Hippocampus
	Hipp_R_2_2	R	Subcortical Nuclei	Hippocampus	Caudal Hippocampus
	IFG_L_6_1	L	Frontal	Inferior Frontal Gyrus	Dorsal Area 44
	IFG_L_6_2	L	Frontal	Inferior Frontal Gyrus	Inferior Frontal Sulcus
	IFG_L_6_3	L	Frontal	Inferior Frontal Gyrus	Caudal Area 45
	IFG_L_6_4	L	Frontal	Inferior Frontal Gyrus	Rostral Area 45
	IFG_L_6_5	L	Frontal	Inferior Frontal Gyrus	Opercular Area 44
	IFG_L_6_6	L	Frontal	Inferior Frontal Gyrus	Ventral Area 44
	IFG_R_6_1	R	Frontal	Inferior Frontal Gyrus	Dorsal Area 44
	IFG_R_6_2	R	Frontal	Inferior Frontal Gyrus	Inferior Frontal Sulcus
	IFG_R_6_3	R	Frontal	Inferior Frontal Gyrus	Caudal Area 45
	IFG_R_6_4	R	Frontal	Inferior Frontal Gyrus	Rostral Area 45
	IFG_R_6_5	R	Frontal	Inferior Frontal Gyrus	Opercular Area 44
	IFG_R_6_6	R	Frontal	Inferior Frontal Gyrus	Ventral Area 44
	INS_L_6_1	L	Insula	Insular Gyrus	Hypergranular Insula
	INS_L_6_2	L	Insula	Insular Gyrus	Ventral Agranular Insula
	INS_L_6_3	L	Insula	Insular Gyrus	Dorsal Agranular Insula
	INS_L_6_4	L	Insula	Insular Gyrus	Ventral Dysgranula, Granular Insula
	INS_L_6_5	L	Insula	Insular Gyrus	Dorsal Granular Insula
	INS_L_6_6	L	Insula	Insular Gyrus	Dorsal Dysgranular Insula
	INS_R_6_1	R	Insula	Insular Gyrus	Hypergranular Insula

	INS_R_6_2	R	Insula	Insular Gyrus	Ventral Agranular Insula
	INS_R_6_3	R	Insula	Insular Gyrus	Dorsal Agranular Insula
	INS_R_6_4	R	Insula	Insular Gyrus	Ventral Dysgranula, Granular Insula
	INS_R_6_5	R	Insula	Insular Gyrus	Dorsal Granular Insula
	INS_R_6_6	R	Insula	Insular Gyrus	Dorsal Dysgranular Insula
	IPL_L_6_2	L	Parietal	Inferior Parietal Lobule	Rostrodorsal Area 39
	IPL_L_6_3	L	Parietal	Inferior Parietal Lobule	Rostrodorsal Area 40
	IPL_L_6_4	L	Parietal	Inferior Parietal Lobule	Caudal Area 40
	IPL_L_6_5	L	Parietal	Inferior Parietal Lobule	Rostroventral Area 39
	IPL_L_6_6	L	Parietal	Inferior Parietal Lobule	Rostroventral Area 40
	IPL_R_6_1	R	Parietal	Inferior Parietal Lobule	Caudal Area 39
	IPL_R_6_2	R	Parietal	Inferior Parietal Lobule	Rostrodorsal Area 39
	IPL_R_6_4	R	Parietal	Inferior Parietal Lobule	Caudal Area 40
	IPL_R_6_5	R	Parietal	Inferior Parietal Lobule	Rostroventral Area 39
	IPL_R_6_6	R	Parietal	Inferior Parietal Lobule	Rostroventral Area 40
	ITG_L_7_2	L	Temporal	Inferior Temporal Gyrus	Extreme Lateroventral Area 37
	ITG_L_7_5	L	Temporal	Inferior Temporal Gyrus	Ventrolateral Area 37
	ITG_R_7_2	R	Temporal	Inferior Temporal Gyrus	Extreme Lateroventral Area 37
	ITG_R_7_5	R	Temporal	Inferior Temporal Gyrus	Ventrolateral Area 37
	LOcC_L_4_2	L	Occipital	Lateral Occipital Cortex	Area V5/MT
	LOcC_L_4_4	L	Occipital	Lateral Occipital Cortex	Inferior Occipital Gyrus
	LOcC_R_4_2	R	Occipital	Lateral Occipital Cortex	Area V5/MT
	LOcC_R_4_4	R	Occipital	Lateral Occipital Cortex	Inferior Occipital Gyrus
	MFG_L_7_2	L	Frontal	Middle Frontal Gyrus	Inferior Frontal Junction
	MFG_L_7_3	L	Frontal	Middle Frontal Gyrus	Area 46
	MFG_L_7_4	L	Frontal	Middle Frontal Gyrus	Ventral Area 9/46
	MFG_L_7_5	L	Frontal	Middle Frontal Gyrus	Ventrolateral Area 8
	MFG_L_7_6	L	Frontal	Middle Frontal Gyrus	Ventrolateral Area 6
	MFG_R_7_2	R	Frontal	Middle Frontal Gyrus	Inferior Frontal Junction
	MFG_R_7_4	R	Frontal	Middle Frontal Gyrus	Ventral Area 9/46
	MFG_R_7_5	R	Frontal	Middle Frontal Gyrus	Ventrolateral Area 8
	MTG_L_4_3	L	Temporal	Middle Temporal Gyrus	Dorsolateral Area 37
	MTG_L_4_4	L	Temporal	Middle Temporal Gyrus	Anterior Superior Temporal Sulcus
	MTG_R_4_3	R	Temporal	Middle Temporal Gyrus	Dorsolateral Area 37
	MTG_R_4_4	R	Temporal	Middle Temporal Gyrus	Anterior Superior Temporal Sulcus
	OrG_L_6_1	L	Frontal	Orbital Gyrus	Medial Area 14
	OrG_L_6_2	L	Frontal	Orbital Gyrus	Orbital Area 12/47
	OrG_L_6_3	L	Frontal	Orbital Gyrus	Lateral Area 11
	OrG_L_6_5	L	Frontal	Orbital Gyrus	Area 13
	OrG_L_6_6	L	Frontal	Orbital Gyrus	Lateral Area 12/47
	OrG_R_6_1	R	Frontal	Orbital Gyrus	Medial Area 14
	OrG_R_6_2	R	Frontal	Orbital Gyrus	Orbital Area 12/47
	OrG_R_6_5	R	Frontal	Orbital Gyrus	Area 13
	OrG_R_6_6	R	Frontal	Orbital Gyrus	Lateral Area 12/47
	PCun_L_4_4	L	Parietal	Precuneus	Area 31
	PCun_R_4_4	R	Parietal	Precuneus	Area 31
	PhG_L_6_3	L	Temporal	Parahippocampal Gyrus	Posterior Parahippocampal Gyrus
	PhG_L_6_5	L	Temporal	Parahippocampal Gyrus	Area Ti
	PhG_L_6_6	L	Temporal	Parahippocampal Gyrus	Area Th (Medial PPHC)
	PhG_R_6_3	R	Temporal	Parahippocampal Gyrus	Posterior Parahippocampal Gyrus
	PhG_R_6_6	R	Temporal	Parahippocampal Gyrus	Area Th (Medial PPHC)
	PoG_L_4_2	L	Parietal	Postcentral Gyrus	Area 1/2/3(Tongue And Larynx)
	PoG_R_4_2	R	Parietal	Postcentral Gyrus	Area 1/2/3(Tongue And Larynx)
	PrG_L_6_5	L	Frontal	Precentral Gyrus	Area 4 (Tongue, Larynx)
	PrG_L_6_6	L	Frontal	Precentral Gyrus	Caudal Ventrolateral Area 6
	PrG_R_6_5	R	Frontal	Precentral Gyrus	Area 4 (Tongue, Larynx)
	PrG_R_6_6	R	Frontal	Precentral Gyrus	Caudal Ventrolateral Area 6
	pSTS_L_2_1	L	Temporal	Superior Temporal Sulcus	Rostroposterior Superior Temporal Sulcus

	pSTS_L_2_2	L	Temporal	Superior Temporal Sulcus	Caudoposterior Superior Temporal Sulcus
	pSTS_R_2_1	R	Temporal	Superior Temporal Sulcus	Rostroposterior Superior Temporal Sulcus
	pSTS_R_2_2	R	Temporal	Superior Temporal Sulcus	Caudoposterior Superior Temporal Sulcus
	SFG_L_7_1	L	Frontal	Superior Frontal Gyrus	Medial Area 8
	SFG_L_7_3	L	Frontal	Superior Frontal Gyrus	Lateral Area 9
	SFG_L_7_5	L	Frontal	Superior Frontal Gyrus	Medial Area 6
	SFG_L_7_6	L	Frontal	Superior Frontal Gyrus	Medial Area 9
	SFG_L_7_7	L	Frontal	Superior Frontal Gyrus	A10M, Medial Area 10
	SFG_R_7_1	R	Frontal	Superior Frontal Gyrus	Medial Area 8
	SFG_R_7_6	R	Frontal	Superior Frontal Gyrus	Medial Area 9
	SFG_R_7_7	R	Frontal	Superior Frontal Gyrus	A10M, Medial Area 10
	SPL_L_5_3	L	Parietal	Superior Parietal Lobule	Lateral Area 5
	SPL_L_5_5	L	Parietal	Superior Parietal Lobule	Intraparietal Area 7
	SPL_R_5_5	R	Parietal	Superior Parietal Lobule	Intraparietal Area 7
	STG_L_6_2	L	Temporal	Superior Temporal Gyrus	Area 41/42
	STG_L_6_3	L	Temporal	Superior Temporal Gyrus	Te
	STG_L_6_4	L	Temporal	Superior Temporal Gyrus	Caudal Area 22
	STG_L_6_5	L	Temporal	Superior Temporal Gyrus	Lateral Area 38
	STG_L_6_6	L	Temporal	Superior Temporal Gyrus	Rostral Area 22
	STG_R_6_2	R	Temporal	Superior Temporal Gyrus	Area 41/42
	STG_R_6_3	R	Temporal	Superior Temporal Gyrus	Te
	STG_R_6_4	R	Temporal	Superior Temporal Gyrus	Caudal Area 22
	STG_R_6_5	R	Temporal	Superior Temporal Gyrus	Lateral Area 38
	STG_R_6_6	R	Temporal	Superior Temporal Gyrus	Rostral Area 22
	Tha_L_8_1	L	Subcortical Nuclei	Thalamus	Medial Prefrontal Thalamus
	Tha_L_8_2	L	Subcortical Nuclei	Thalamus	Premotor Thalamus
	Tha_L_8_3	L	Subcortical Nuclei	Thalamus	Sensory Thalamus
	Tha_L_8_4	L	Subcortical Nuclei	Thalamus	Rostral Temporal Thalamus
	Tha_L_8_5	L	Subcortical Nuclei	Thalamus	Posterior Parietal Thalamus
	Tha_L_8_6	L	Subcortical Nuclei	Thalamus	Occipital Thalamus
	Tha_L_8_7	L	Subcortical Nuclei	Thalamus	Caudal Temporal Thalamus
	Tha_L_8_8	L	Subcortical Nuclei	Thalamus	Lateral Prefrontal Thalamus
	Tha_R_8_1	R	Subcortical Nuclei	Thalamus	Medial Prefrontal Thalamus
	Tha_R_8_2	R	Subcortical Nuclei	Thalamus	Premotor Thalamus
	Tha_R_8_3	R	Subcortical Nuclei	Thalamus	Sensory Thalamus
	Tha_R_8_4	R	Subcortical Nuclei	Thalamus	Rostral Temporal Thalamus
	Tha_R_8_5	R	Subcortical Nuclei	Thalamus	Posterior Parietal Thalamus
	Tha_R_8_6	R	Subcortical Nuclei	Thalamus	Occipital Thalamus
	Tha_R_8_7	R	Subcortical Nuclei	Thalamus	Caudal Temporal Thalamus
	Tha_R_8_8	R	Subcortical Nuclei	Thalamus	Lateral Prefrontal Thalamus
Language	Amyg_L_2_1	L	Subcortical Nuclei	Amygdala	Medial Amygdala
	Amyg_L_2_2	L	Subcortical Nuclei	Amygdala	Lateral Amygdala
	Amyg_R_2_2	R	Subcortical Nuclei	Amygdala	Lateral Amygdala
	BG_L_6_1	L	Subcortical Nuclei	Basal Ganglia	Ventral Caudate
	BG_L_6_2	L	Subcortical Nuclei	Basal Ganglia	Globus Pallidus
	BG_L_6_4	L	Subcortical Nuclei	Basal Ganglia	Ventromedial Putamen
	BG_L_6_5	L	Subcortical Nuclei	Basal Ganglia	Dorsal Caudate
	BG_L_6_6	L	Subcortical Nuclei	Basal Ganglia	Dorsolateral Putamen
	BG_R_6_1	R	Subcortical Nuclei	Basal Ganglia	Ventral Caudate
	BG_R_6_2	R	Subcortical Nuclei	Basal Ganglia	Globus Pallidus
	BG_R_6_4	R	Subcortical Nuclei	Basal Ganglia	Ventromedial Putamen
	BG_R_6_5	R	Subcortical Nuclei	Basal Ganglia	Dorsal Caudate
	CG_L_7_1	L	Cingulate	Cingulate Gyrus	Dorsal Area 23
	CG_L_7_5	L	Cingulate	Cingulate Gyrus	Caudodorsal Area 24
	CG_R_7_1	R	Cingulate	Cingulate Gyrus	Dorsal Area 23
	CG_R_7_3	R	Cingulate	Cingulate Gyrus	Pregenual Area 32
	CG_R_7_5	R	Cingulate	Cingulate Gyrus	Caudodorsal Area 24
	FuG_L_3_2	L	Temporal	Fusiform Gyrus	Medioventral Area37

	FuG_L_3_3	L	Temporal	Fusiform Gyrus	Lateroventral Area37
	FuG_R_3_2	R	Temporal	Fusiform Gyrus	Medioventral Area37
	FuG_R_3_3	R	Temporal	Fusiform Gyrus	Lateroventral Area37
	IFG_L_6_1	L	Frontal	Inferior Frontal Gyrus	Dorsal Area 44
	IFG_L_6_2	L	Frontal	Inferior Frontal Gyrus	Inferior Frontal Sulcus
	IFG_L_6_3	L	Frontal	Inferior Frontal Gyrus	Caudal Area 45
	IFG_L_6_4	L	Frontal	Inferior Frontal Gyrus	Rostral Area 45
	IFG_L_6_5	L	Frontal	Inferior Frontal Gyrus	Opercular Area 44
	IFG_L_6_6	L	Frontal	Inferior Frontal Gyrus	Ventral Area 44
	IFG_R_6_1	R	Frontal	Inferior Frontal Gyrus	Dorsal Area 44
	IFG_R_6_2	R	Frontal	Inferior Frontal Gyrus	Inferior Frontal Sulcus
	IFG_R_6_3	R	Frontal	Inferior Frontal Gyrus	Caudal Area 45
	IFG_R_6_4	R	Frontal	Inferior Frontal Gyrus	Rostral Area 45
	IFG_R_6_5	R	Frontal	Inferior Frontal Gyrus	Opercular Area 44
	IFG_R_6_6	R	Frontal	Inferior Frontal Gyrus	Ventral Area 44
	INS_L_6_1	L	Insula	Insular Gyrus	Hypergranular Insula
	INS_L_6_2	L	Insula	Insular Gyrus	Ventral Agranular Insula
	INS_L_6_3	L	Insula	Insular Gyrus	Dorsal Agranular Insula
	INS_L_6_6	L	Insula	Insular Gyrus	Dorsal Dysgranular Insula
	INS_R_6_2	R	Insula	Insular Gyrus	Ventral Agranular Insula
	INS_R_6_3	R	Insula	Insular Gyrus	Dorsal Agranular Insula
	INS_R_6_6	R	Insula	Insular Gyrus	Dorsal Dysgranular Insula
	IPL_L_6_2	L	Parietal	Inferior Parietal Lobule	Rostrodorsal Area 39
	IPL_L_6_3	L	Parietal	Inferior Parietal Lobule	Rostrodorsal Area 40
	IPL_L_6_4	L	Parietal	Inferior Parietal Lobule	Caudal Area 40
	IPL_L_6_5	L	Parietal	Inferior Parietal Lobule	Rostroventral Area 39
	IPL_L_6_6	L	Parietal	Inferior Parietal Lobule	Rostroventral Area 40
	IPL_R_6_2	R	Parietal	Inferior Parietal Lobule	Rostrodorsal Area 39
	IPL_R_6_3	R	Parietal	Inferior Parietal Lobule	Rostrodorsal Area 40
	IPL_R_6_4	R	Parietal	Inferior Parietal Lobule	Caudal Area 40
	IPL_R_6_5	R	Parietal	Inferior Parietal Lobule	Rostroventral Area 39
	ITG_L_7_2	L	Temporal	Inferior Temporal Gyrus	Extreme Lateroventral Area 37
	ITG_L_7_5	L	Temporal	Inferior Temporal Gyrus	Ventrolateral Area 37
	ITG_L_7_6	L	Temporal	Inferior Temporal Gyrus	Caudolateral of Area 20
	ITG_R_7_5	R	Temporal	Inferior Temporal Gyrus	Ventrolateral Area 37
	LOcC_L_2_2	L	Occipital	Lateral Occipital Cortex	Lateral Superior Occipital Gyrus
	LOcC_L_4_1	L	Occipital	Lateral Occipital Cortex	Middle Occipital Gyrus
	LOcC_L_4_2	L	Occipital	Lateral Occipital Cortex	Area V5/MT
	LOcC_L_4_3	L	Occipital	Lateral Occipital Cortex	Occipital Polar Cortex
	LOcC_L_4_4	L	Occipital	Lateral Occipital Cortex	Inferior Occipital Gyrus
	LOcC_R_4_1	R	Occipital	Lateral Occipital Cortex	Middle Occipital Gyrus
	LOcC_R_4_2	R	Occipital	Lateral Occipital Cortex	Area V5/MT
	LOcC_R_4_3	R	Occipital	Lateral Occipital Cortex	Occipital Polar Cortex
	LOcC_R_4_4	R	Occipital	Lateral Occipital Cortex	Inferior Occipital Gyrus
	MFG_L_7_2	L	Frontal	Middle Frontal Gyrus	Inferior Frontal Junction
	MFG_L_7_4	L	Frontal	Middle Frontal Gyrus	Ventral Area 9/46
	MFG_L_7_6	L	Frontal	Middle Frontal Gyrus	Ventrolateral Area 6
	MFG_R_7_2	R	Frontal	Middle Frontal Gyrus	Inferior Frontal Junction
	MFG_R_7_4	R	Frontal	Middle Frontal Gyrus	Ventral Area 9/46
	MFG_R_7_5	R	Frontal	Middle Frontal Gyrus	Ventrolateral Area 8
	MFG_R_7_6	R	Frontal	Middle Frontal Gyrus	Ventrolateral Area 6
	MTG_L_4_1	L	Temporal	Middle Temporal Gyrus	Caudal Area 21
	MTG_L_4_2	L	Temporal	Middle Temporal Gyrus	Rostral Area 21
	MTG_L_4_3	L	Temporal	Middle Temporal Gyrus	Dorsolateral Area 37
	MTG_L_4_4	L	Temporal	Middle Temporal Gyrus	Anterior Superior Temporal Sulcus
	MTG_R_4_3	R	Temporal	Middle Temporal Gyrus	Dorsolateral Area 37
	MTG_R_4_4	R	Temporal	Middle Temporal Gyrus	Anterior Superior Temporal Sulcus
	MVOcC_L_5_3	L	Occipital	Ventral Occipital Cortex	Caudal Cuneus Gyrus

	MVOcC_R_5_1	R	Occipital	Ventral Occipital Cortex	Caudal Lingual Gyrus
	MVOcC_R_5_2	R	Occipital	Ventral Occipital Cortex	Rostral Cuneus Gyrus
	MVOcC_R_5_3	R	Occipital	Ventral Occipital Cortex	Caudal Cuneus Gyrus
	OrG_L_6_2	L	Frontal	Orbital Gyrus	Orbital Area 12/47
	OrG_L_6_6	L	Frontal	Orbital Gyrus	Lateral Area 12/47
	OrG_R_6_2	R	Frontal	Orbital Gyrus	Orbital Area 12/47
	OrG_R_6_6	R	Frontal	Orbital Gyrus	Lateral Area 12/47
	PCun_L_4_1	L	Parietal	Precuneus	Medial Area 7
	PCun_L_4_4	L	Parietal	Precuneus	Area 31
	PCun_R_4_4	R	Parietal	Precuneus	Area 31
	PhG_L_6_3	L	Temporal	Parahippocampal Gyrus	Posterior Parahippocampal Gyrus
	PoG_L_4_1	L	Parietal	Postcentral Gyrus	Area 1/2/3 (Upper Limb, Head, Face)
	PoG_L_4_2	L	Parietal	Postcentral Gyrus	Area 1/2/3(Tongue And Larynx)
	PoG_L_4_3	L	Parietal	Postcentral Gyrus	Area 2
	PoG_R_4_2	R	Parietal	Postcentral Gyrus	Area 1/2/3(Tongue And Larynx)
	PrG_L_6_1	L	Frontal	Precentral Gyrus	Area 4 (Head, Face)
	PrG_L_6_2	L	Frontal	Precentral Gyrus	Caudal Dorsolateral Area 6
	PrG_L_6_5	L	Frontal	Precentral Gyrus	Area 4 (Tongue, Larynx)
	PrG_L_6_6	L	Frontal	Precentral Gyrus	Caudal Ventrolateral Area 6
	PrG_R_6_1	R	Frontal	Precentral Gyrus	Area 4 (Head, Face)
	PrG_R_6_2	R	Frontal	Precentral Gyrus	Caudal Dorsolateral Area 6
	PrG_R_6_5	R	Frontal	Precentral Gyrus	Area 4 (Tongue, Larynx)
	PrG_R_6_6	R	Frontal	Precentral Gyrus	Caudal Ventrolateral Area 6
	pSTS_L_2_1	L	Temporal	Superior Temporal Sulcus	Rostroposterior Superior Temporal Sulcus
	pSTS_L_2_2	L	Temporal	Superior Temporal Sulcus	Caudoposterior Superior Temporal Sulcus
	pSTS_R_2_1	R	Temporal	Superior Temporal Sulcus	Rostroposterior Superior Temporal Sulcus
	pSTS_R_2_2	R	Temporal	Superior Temporal Sulcus	Caudoposterior Superior Temporal Sulcus
	SFG_L_7_1	L	Frontal	Superior Frontal Gyrus	Medial Area 8
	SFG_L_7_3	L	Frontal	Superior Frontal Gyrus	Lateral Area 9
	SFG_L_7_4	L	Frontal	Superior Frontal Gyrus	Dorsolateral Area 6
	SFG_L_7_5	L	Frontal	Superior Frontal Gyrus	Medial Area 6
	SFG_L_7_6	L	Frontal	Superior Frontal Gyrus	Medial Area 9
	SFG_R_7_1	R	Frontal	Superior Frontal Gyrus	Medial Area 8
	SFG_R_7_5	R	Frontal	Superior Frontal Gyrus	Medial Area 6
	SFG_R_7_6	R	Frontal	Superior Frontal Gyrus	Medial Area 9
	SPL_L_5_2	L	Parietal	Superior Parietal Lobule	Caudal Area 7
	SPL_L_5_3	L	Parietal	Superior Parietal Lobule	Lateral Area 5
	SPL_L_5_5	L	Parietal	Superior Parietal Lobule	Intraparietal Area 7
	SPL_R_5_3	R	Parietal	Superior Parietal Lobule	Lateral Area 5
	SPL_R_5_5	R	Parietal	Superior Parietal Lobule	Intraparietal Area 7
	STG_L_6_2	L	Temporal	Superior Temporal Gyrus	Area 41/42
	STG_L_6_3	L	Temporal	Superior Temporal Gyrus	Te
	STG_L_6_4	L	Temporal	Superior Temporal Gyrus	Caudal Area 22
	STG_L_6_5	L	Temporal	Superior Temporal Gyrus	Lateral Area 38
	STG_L_6_6	L	Temporal	Superior Temporal Gyrus	Rostral Area 22
	STG_R_6_2	R	Temporal	Superior Temporal Gyrus	Area 41/42
	STG_R_6_3	R	Temporal	Superior Temporal Gyrus	Te
	STG_R_6_4	R	Temporal	Superior Temporal Gyrus	Caudal Area 22
	STG_R_6_5	R	Temporal	Superior Temporal Gyrus	Lateral Area 38
	STG_R_6_6	R	Temporal	Superior Temporal Gyrus	Rostral Area 22
	Tha_L_8_1	L	Subcortical Nuclei	Thalamus	Medial Prefrontal Thalamus
	Tha_L_8_2	L	Subcortical Nuclei	Thalamus	Premotor Thalamus
	Tha_L_8_3	L	Subcortical Nuclei	Thalamus	Sensory Thalamus
	Tha_L_8_4	L	Subcortical Nuclei	Thalamus	Rostral Temporal Thalamus
	Tha_L_8_5	L	Subcortical Nuclei	Thalamus	Posterior Parietal Thalamus
	Tha_L_8_6	L	Subcortical Nuclei	Thalamus	Occipital Thalamus
	Tha_L_8_7	L	Subcortical Nuclei	Thalamus	Caudal Temporal Thalamus
	Tha_L_8_8	L	Subcortical Nuclei	Thalamus	Lateral Prefrontal Thalamus

	Tha_R_8_1	R	Subcortical Nuclei	Thalamus	Medial Prefrontal Thalamus
	Tha_R_8_2	R	Subcortical Nuclei	Thalamus	Premotor Thalamus
	Tha_R_8_3	R	Subcortical Nuclei	Thalamus	Sensory Thalamus
	Tha_R_8_4	R	Subcortical Nuclei	Thalamus	Rostral Temporal Thalamus
	Tha_R_8_5	R	Subcortical Nuclei	Thalamus	Posterior Parietal Thalamus
	Tha_R_8_7	R	Subcortical Nuclei	Thalamus	Caudal Temporal Thalamus
	Tha_R_8_8	R	Subcortical Nuclei	Thalamus	Lateral Prefrontal Thalamus

Supplemental Table S3: Hyperparameters optimized during randomized search for each model. All optimizations were implemented with *RandomizedSearchCV* within *SciKit-Learn.* All distributions were generated using *SciPy* and all continuous values included were greater than zero.

Algorithm	*SciKit-Learn* Package	Hyperparameter	Sampling Distribution
Gradient Boosting Machine	GradientBoostingRegressor	learning_rate	Gaussian (loc=0.0, scale=0.1)
		n_estimators	Gaussian (loc=500, scale=300; rounded to nearest integer)
		max_features	Gaussian (loc=62, scale=62; rounded to nearest integer)
		subsample	Gaussian (loc=1.0, scale=0.25)
		criterion	{'friedman_mse', 'mse'}
		max_depth	Gaussian (loc=2.5, scale=2.5; rounded to nearest integer)
Ridge Regression	SDGRegressor	learning_rate	{'optimal', 'invscaling', 'adaptive'}
		alpha	Gaussian (loc=0.0, scale=0.1)
		tol	Gaussian (loc=0.001, scale=0.1)
		power_t	Gaussian (loc=0.5, scale=0.1)
		eta0	Gaussian (loc=0.0, scale=0.1)
Multilayer Perceptron	MLPRegressor	learning_rate_init	Gaussian (loc=0.0, scale=0.1)
		alpha	Gaussian (loc=0.0, scale=0.1)
		tol	Gaussian (loc=0.001, scale=0.1)
		power_t	Gaussian (loc=0.5, scale=0.1)
		solvers	{'lbfgs', 'adam'}
Support Vector Machine	SVR	C	Gaussian (loc=0.0, scale=1.0)
		tol	Gaussian (loc=0.0, scale=0.1)
		degree	{'1', '2', '3', '4', '5'}
		kernel	{'poly', 'rbf'}
		gamma	Gaussian (loc=0.0, scale=1.0)
		coef0	Gaussian (loc=0.0, scale=5.0)
		epsilon	Gaussian (loc=0.0, scale=0.5)
Random Forest	RandomForestRegressor	n_estimators	Gaussian (loc=500, scale=300; rounded to nearest integer)
		max_features	Gaussian (loc=62, scale=62; rounded to nearest integer)

Supplemental Table S4. Model algorithm performances on the evaluation set of typically-developing girls. Above-chance performance is calculated by subtracting the optimized performance and average performance when predicting randomized label vectors. Coefficients and *p*-values correspond to results from Pearson correlation tests between predicted age and chronological age.

Neural Feature Set	Algorithm	Mean Absolute Error (years)	Above-Chance Performance (years)	Pearson Coefficient (r)	p
Whole-Brain	Super Learner	1.666	1.003	0.677	< 0.001
	Random Forest	1.812	0.272	0.434	0.030
	Support Vector Machine	2.277	0.865	0.658	< 0.001
	Ridge Regression	2.484	0.972	0.657	< 0.001
	Gradient Boosting Machine	1.824	0.560	0.520	0.008
	Multilayer Perceptron	3.914	0.162	0.264	0.202
Emotion Circuitry	Super Learner	1.602	0.632	0.663	< 0.001
	Random Forest	1.658	0.403	0.539	0.005
	Support Vector Machine	1.848	0.529	0.584	0.002
	Ridge Regression	2.036	0.976	0.660	< 0.001
	Gradient Boosting Machine	1.613	0.517	0.549	0.005
	Multilayer Perceptron	2.099	1.034	0.638	< 0.001
Language Circuitry	Super Learner	1.569	1.110	0.655	< 0.001
	Random Forest	1.747	0.340	0.486	0.014
	Support Vector Machine	2.300	0.996	0.663	< 0.001
	Ridge Regression	2.327	0.975	0.656	< 0.001
	Gradient Boosting Machine	1.841	0.763	0.585	0.002
	Multilayer Perceptron	3.416	0.394	0.441	0.027

SUPPLEMENTAL FIGURES AND LEGENDS

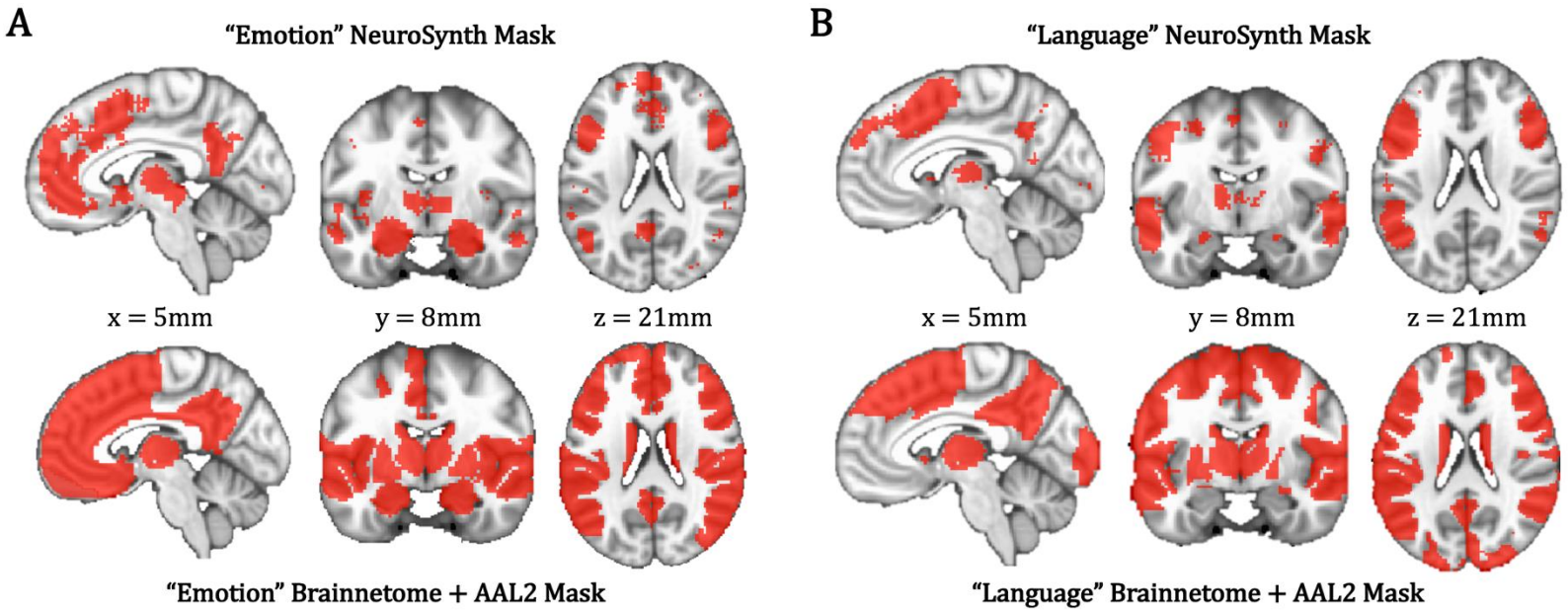

Supplemental Figure S1. Masks taken from the NeuroSynth neuroimaging meta-analysis database using the terms **(A)** "emotion" and **(B)** "language". The uniformity test was used to err on the side of voxel inclusion. Below each NeuroSynth mask is the corresponding mask of the cortical/subcortical and cerebellar ROIs from the Brainnetome and AAL2 atlases respectively. Values for x, y, and z refer to slices in the volume. ROI = region of interest; AAL = automated anatomical labelling.

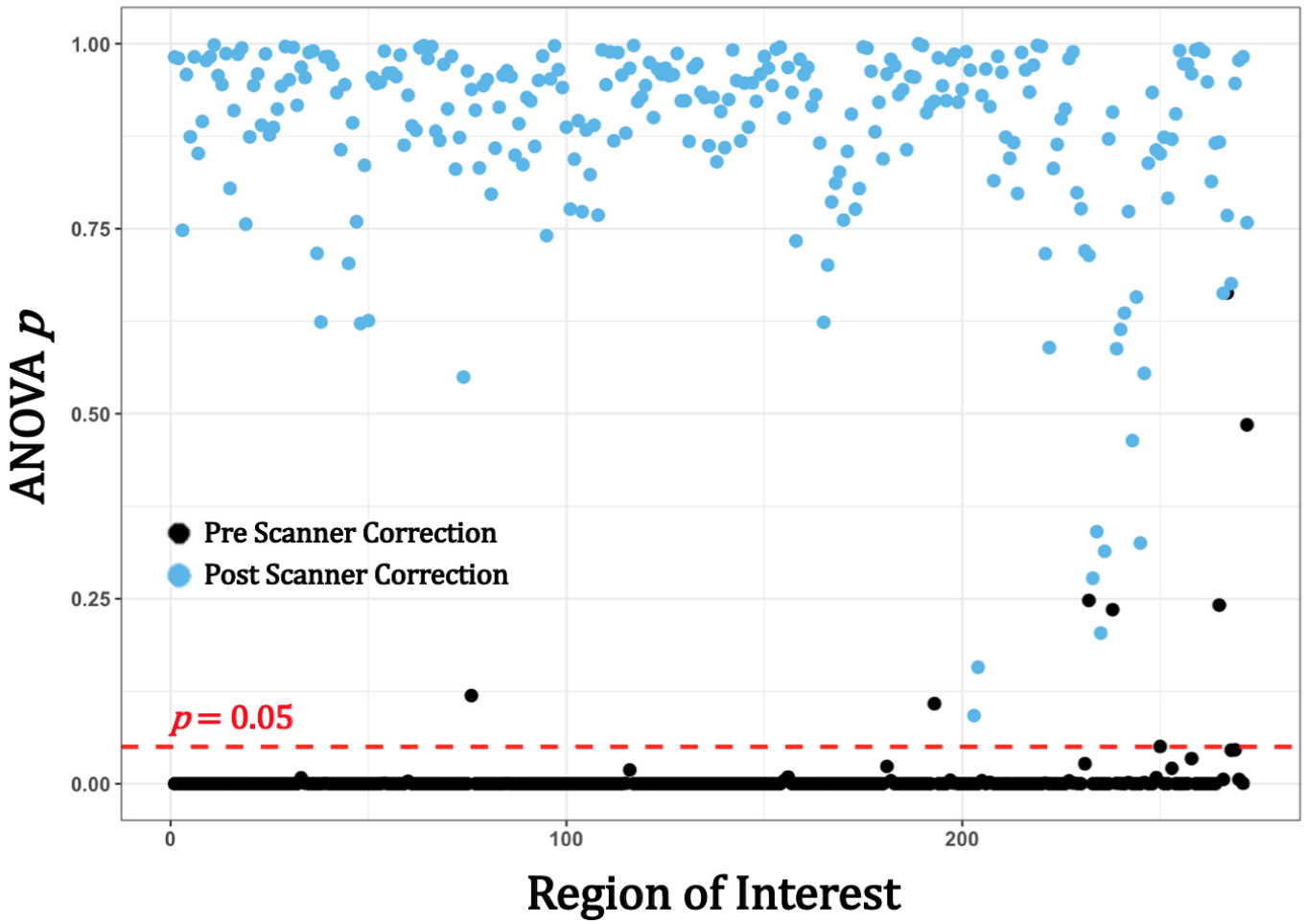

Supplemental Figure S2. The results of batch correction across GMV estimates through *Combat*. For each GMV region of interest, the *p*-value associated with the *F*-statistic from a one-way analysis of variance (low *p*'s indicate at least one significant difference in average GMV across MR scanners). GMV = gray matter volume; MR = magnetic resonance

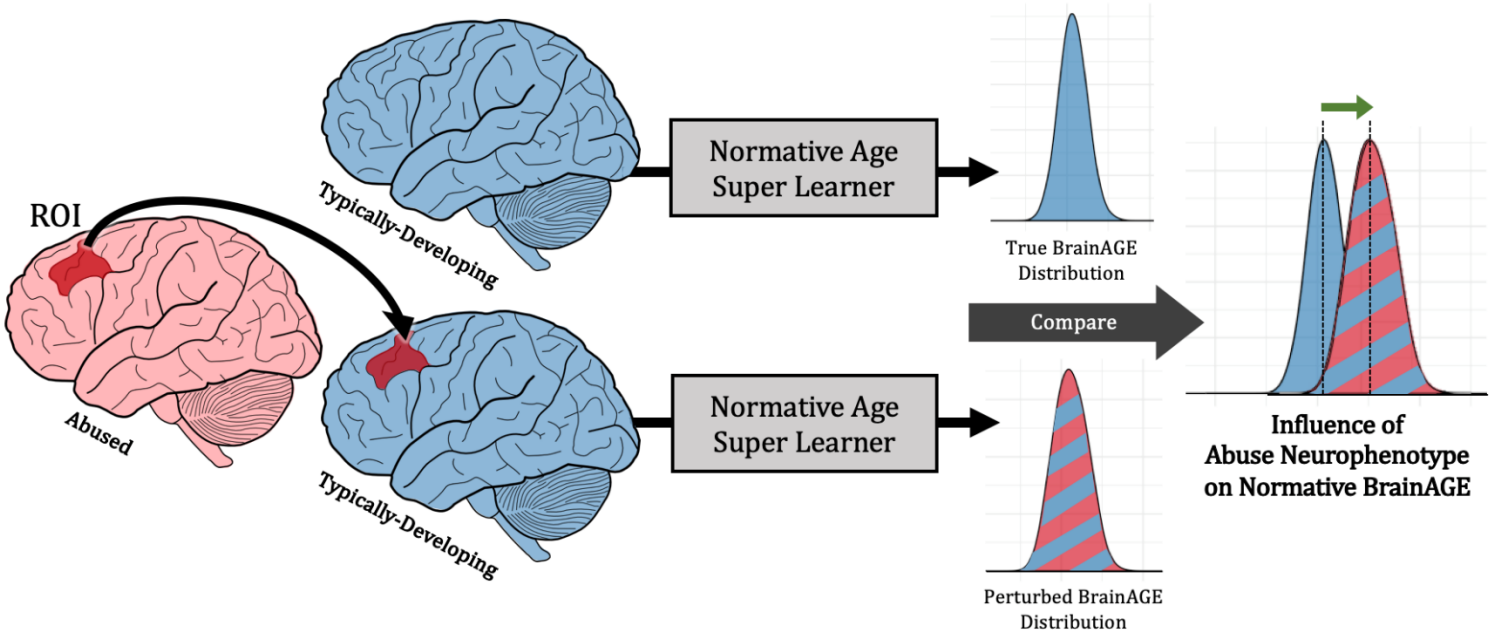

Supplemental Figure S3. Simplified schematic of the perturbation sensitivity algorithm used to determine feature influence on BrainAGE distributions. The algorithm was run for each ROI including 1000 simulations. First, the true distribution of BrainAGEs was calculated using the true, non-perturbed feature set (only occurred on the first simulation). Next, an abuse-perturbed feature set was created by generating a random bootstrap sample of each abuse-related ROI (Resilient and Susceptible). The abuse-related bootstrap replaces the existing ROI in the TD feature set and BrainAGEs are recalculated. Median perturbed BrainAGE was calculated across simulations for each participant. Two-sample Wilcoxon Tests were used to compare the abuse-perturbed BrainAGE distribution to the true and TD-perturbed BrainAGE distributions. If distributions were significantly different after false discovery rate correction (FDR-$p < 0.05$), that abuse feature was considered significantly influential to BrainAGE. ROI= region-of-interest; BrainAGE = brain age gap estimate; TD = typically-developing

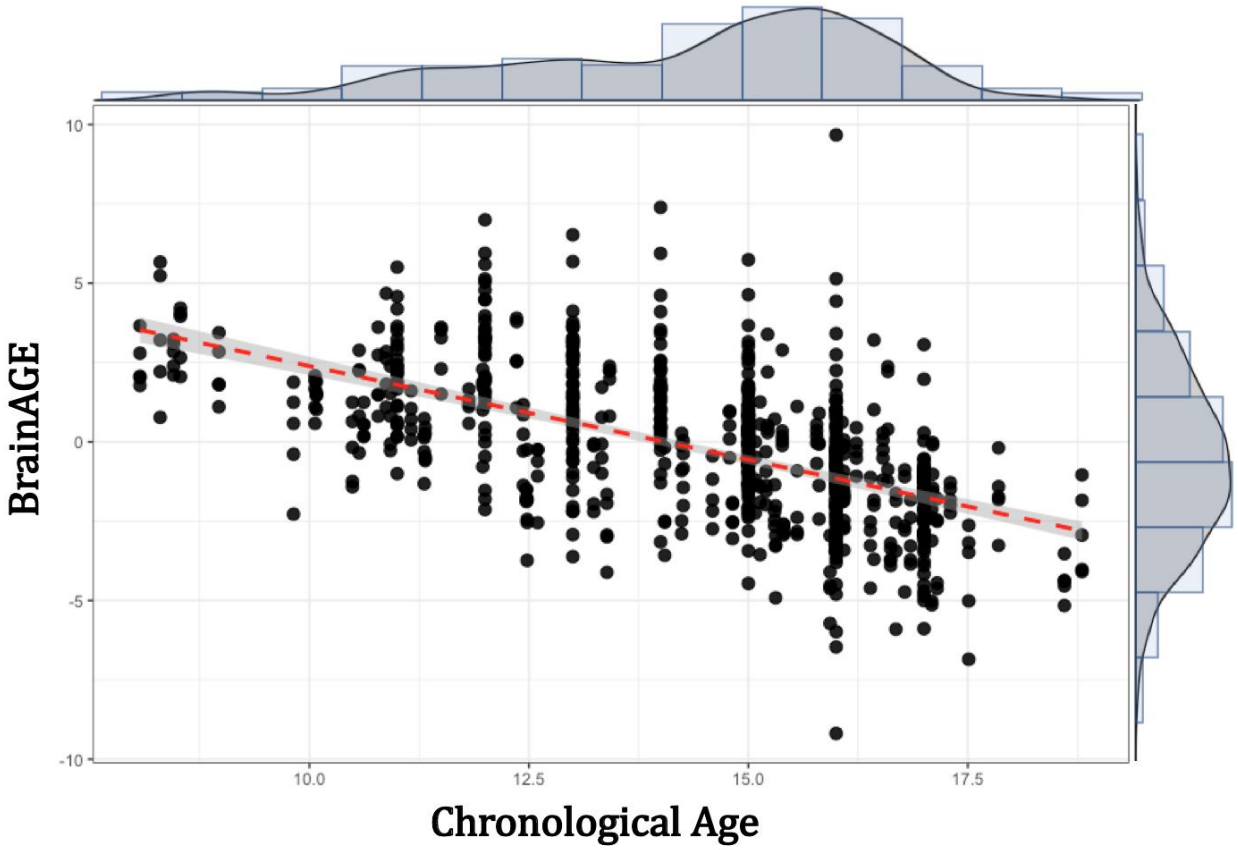

Supplemental Figure S4. Label bias observed across circuits when predicting chronological age.

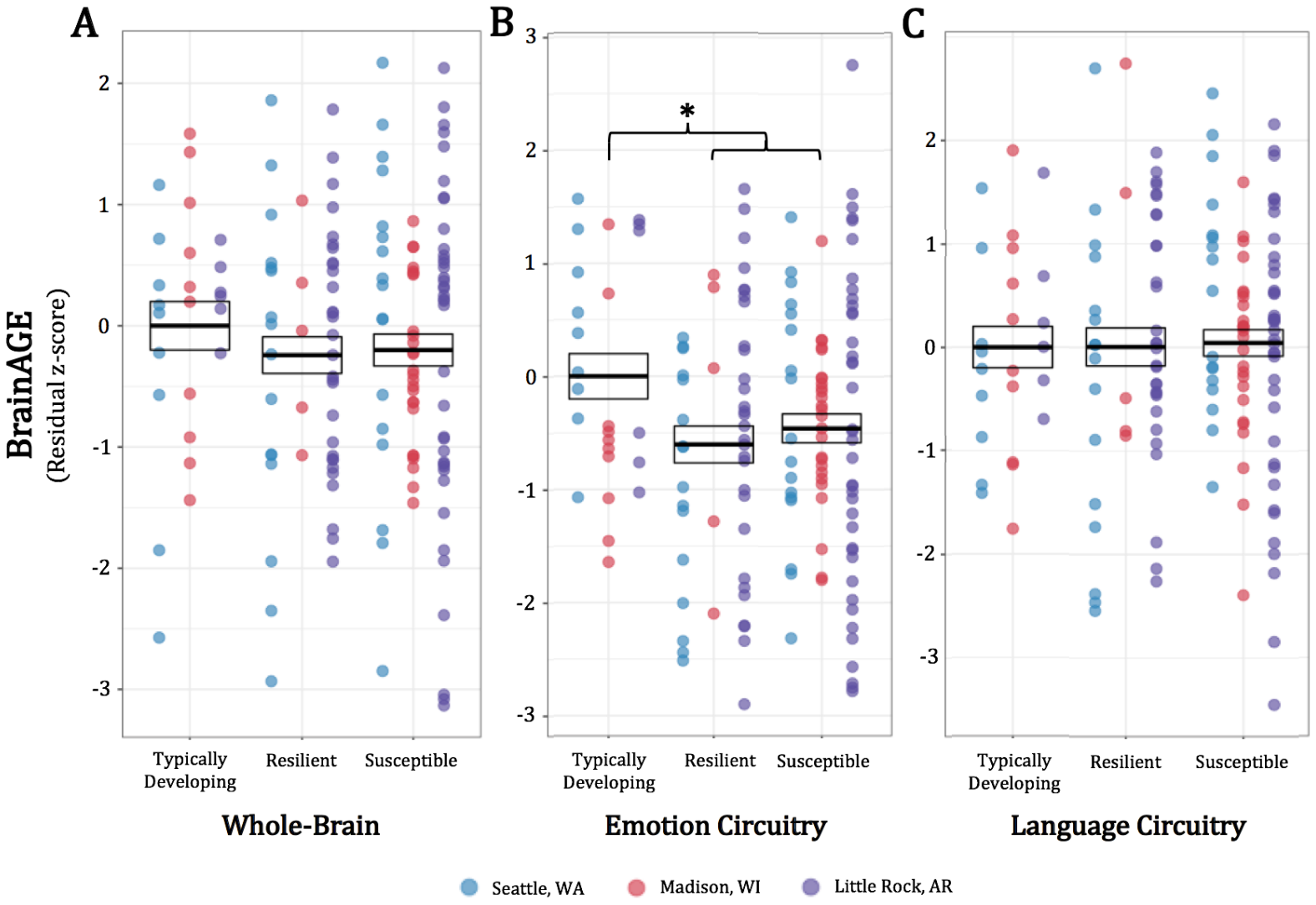

Supplemental Figure S5. Abuse- and internalizing diagnosis-related associations with BrainAGE for whole-brain, emotion circuit, and language circuit feature sets. Colors indicate the MR scanner that each BrainAGE originated from. BrainAGEs are represented as residualized *z*-scores relative to TD girls, controlling for label (chronological age), MR scanner, IQ, and physical neglect. **(A)** For the whole-brain analysis, there were no significant differences in BrainAGE across groups. **(B)** For the emotion circuit analysis, an abuse main effect shows that Resilient and Susceptible girls show significantly reduced average BrainAGE relative to TD girls. **(C)** For the language circuit analysis, there were no significant differences in BrainAGE across groups. BrainAGE = brain age gap estimate; TD = typically-developing; *$p < 0.017$ (after adjustment for experiment-wide Bonferroni correction).

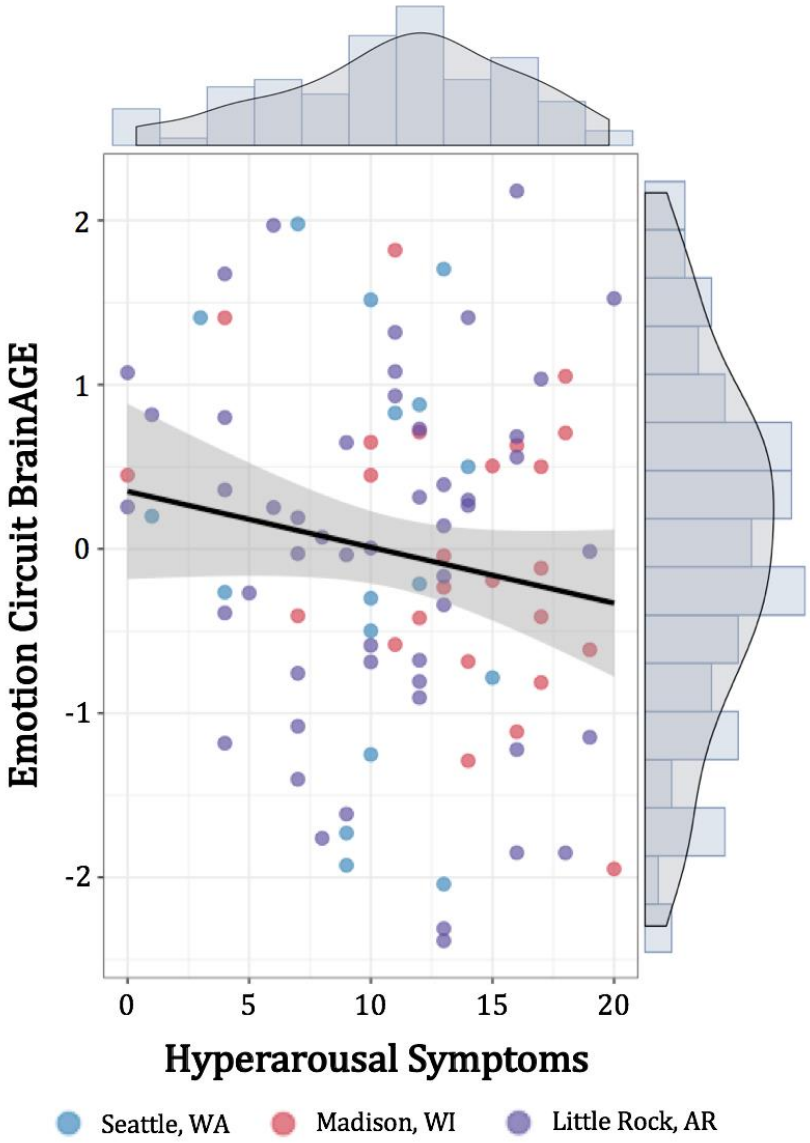

Supplemental Figure S6. Symptom-level association with emotion circuit BrainAGEs across abused girls. Colors indicate the MR scanner that each BrainAGE originated from. Graphed results control for label (chronological age), IQ, MR scanner, physical neglect, and abuse load. Emotion circuitry BrainAGEs were negatively associated with hyperarousal symptoms (PTSD-RI subscore D). BrainAGE = brain age gap estimate; PTSD-RI = Post-Traumatic Stress Disorder Reaction Index.